Article ID: 1006-8775(2023) 02-0153-15

Moisture Sources and Their Contributions to Summer Precipitation in the East of Southwest China

LI Yong-hua (李永华)[1], HUANG Ding-an (黄丁安)[2], LU Chu-han (卢楚翰)[3], XIANG Bo (向 波)[1], ZHOU Jie (周 杰)[1], HE Juan-xiong (何卷雄)[4]

(1. CMA Key Open Laboratory of Transforming Climate Resources to Economy/Chongqing Climate Center, Chongqing 401147 China; 2. School of Atmospheric Sciences, Nanjing University of Information Science and Technology, Nanjing 210044 China; 3. Key Laboratory of Ecosystem Carbon Source and Sink, China Meteorological Administration (ECSS-CMA), Wuxi University, Wuxi, Jiangsu 214063 China; 4. CAS-TWAS Center of Excellence for Climate and Environment Sciences, Beijing 100029 China)

Abstract: Complex topography, special geographical location and sea-land-air interactions lead to high interannual variability of summer precipitation in the east of Southwest China (ESWC). However, the contributions, influencing factors and mechanisms of remote and local evaporation remain to be further investigated. Using clustering analysis and Hybrid Single-Particle Lagrangian Integrated Trajectory version 5 model, we analyze the contributions of remote moisture transport and local evaporation to summer precipitation in the ESWC and their causes. There are mainly five remote moisture channels in the ESWC, namely the Arabian Sea channel, Bay of Bengal channel, western Pacific channel, Northwest channel 1 and Northwest channel 2. Among the five channels, the western Pacific channel has the largest number of trajectories, while the Bay of Bengal channel has the largest contribution rate of specific humidity (33.33%) and moisture flux (33.14%). The amount of regional average precipitation is close to that of the precipitation caused by remote moisture transport, and both are considerably greater than the rainfall amount caused by local evaporation. However, on interannual time scales, precipitation recirculation rates are negatively correlated to regional average precipitation and precipitation caused by remote moisture transport but are consistent with that caused by local evaporation. An apparent "+ − +" wave train can be found on the height anomaly field in East Asia, and the sea surface temperature anomalies are positive in the equatorial Middle-East Pacific, the South China Sea, the Bay of Bengal and the Arabian Sea. These phenomena cause southwest-northeast moisture transport with strong updrafts, thereby resulting in more precipitation in the ESWC.

Key words: east of Southwest China; summer precipitation; moisture sources; local evaporation; contributions of moisture

CLC number: P461 **Document code:** A

Citation: LI Yong-hua, HUANG Ding-an, LU Chu-han, et al. Moisture Sources and Their Contributions to Summer Precipitation in the East of Southwest China [J]. Journal of Tropical Meteorology, 2023, 29(2): 153-167, https://doi.org/10.46267/j.1006-8775.2023.012

1 INTRODUCTION

The east of Southwest China (ESWC), namely the area of 27° − 32° N, 105° − 110° E in this study, covers eastern Sichuan Province, Chongqing Municipality, northern Guizhou Province, western Hunan Province and western Hubei Province. It is located on the east side of the Tibetan Plateau, with a remarkably complex topography and geomorphology. Close to the Pacific Ocean in the east and the Indian Ocean in the southwest, the ESWC is one of the regions with abundant summer precipitation. Due to the special geographical location, the weather and climate in the ESWC are affected by both the Tibetan Plateau and the South Asian (Indian) and East Asian monsoons. In addition, this region is of great concern because its precipitation has a critical impact on the water storage of the Three Gorges Reservoir and it is near the western boundary of the extensive precipitation zone in China. The complex topography, special geographical location and sea-land-air interactions result in high interannual and interdecadal variabilities of summer precipitation in the ESWC (SPE) (Li [1]; Ma and Tan [2]). Therefore, a systematic analysis of the characteristics and causes of the SPE can contribute to improving summer precipitation prediction and help scientific decision-making.

Moisture transport and budget in the atmosphere are crucial in studies on the continuity and change of global atmospheric circulations since moisture is one of the necessary conditions for precipitation. The study of

Received 2022-09-09; **Revised** 2023-02-15; **Accepted** 2023-05-15

Funding: National Natural Science Foundation of China (41875111); Special program for innovation and development of China Meteorological Administration (CXFZ2022J031, CXFZ2021J018); National Natural Science Foundation of China (40975058)

Biography: LI Yong-hua, Ph. D., primarily undertaking research on climate change.

Corresponding author: LU Chu-han, e-mail: luchuhan@nuist.edu.cn

moisture transport can help to reveal the formation of climate and the occurrence and development of weather processes, as well as the basic patterns of hydrological cycles and water balance including atmospheric water, surface water and groundwater (Wu [3]; Zhai and Eskridge [4]; Huang et al. [5]; Zhang [6]; Zhou and Li [7]; He et al. [8]; Zhang et al. [9]; Ryu et al. [10]; Wang et al. [11]; Li et al. [12]; Sun et al. [13]). Numerous studies have suggested that the path and intensity of moisture transport can greatly impact the distribution of the main rainbelts of the summer precipitation in China (Tao et al. [14]; Xie and Dai [15]; Ding and Hu [16]; Xu et al. [17]; Ma and Gao [18]; Jiang et al. [19]; Yang et al. [20]; Chu et al. [21−22]). The variations and anomalies of moisture transport are the direct cause of extreme weather such as droughts, floods and rainstorms in monsoon regions (Li and Jiang [23]; Chen et al. [24]; Ding et al. [25]; Ran et al. [26]; Sun et al. [27]; Bueh et al. [28]). Therefore, studying the variability of moisture transport and its relationship and mechanism with extreme weather and climate events such as droughts and floods can help to improve extreme climate and weather prediction.

Several studies have been conducted to investigate moisture transport in the ESWC and its adjacent areas. Zhou and Li[7] and Zhou et al.[29] analyzed the climatic characteristics of moisture transport in the upper reaches of the Yangtze River, the eastern Tibetan Plateau and its adjacent areas using the long-term moisture transport data vertically integrated from the surface. The results showed that the moisture mainly comes from mid-latitude westerlies in winter and spring and from the Bay of Bengal and the South China Sea in summer. Jiang et al. [30] analyzed the average moisture transport in the Sichuan Basin in summer and the differences in moisture transport between typical drought and flood years in the Sichuan Basin based on the observation data in the summers from 1981 to 2000. They concluded that the summer moisture in the Sichuan Basin mainly comes from the Tibetan Plateau, Bay of Bengal and South China Sea. Li et al. [31] explored the characteristics of summer moisture transport in drought and flood years in the ESWC, and they found two main moisture channels. One is the Tibetan Plateau-Bay of Bengal channel, with moisture entering the ESWC through Myanmar and Yunnan Province. In the other channel, moisture is transported eastward to the Indochina Peninsula and the South China Sea through the southern Bay of Bengal, and then it converges with the moisture carried by cross-equatorial airflows in the South China Sea and turns to the ESWC. The southerly moisture turning from the western side of the Western Pacific subtropical high also affects the moisture transport to the ESWC. Li et al. [32] investigated the influence of moisture transport anomalies over Southwest China using the Hybrid Single-Particle Lagrangian Integrated Trajectory (HYSPLIT) version 4.9. The results indicated that the air masses from the western Pacific, Bay of Bengal or eastern coast of China (in rare cases) carry more moisture, which may cause precipitation in Southwest China. Huang and Cui [33] studied the moisture sources of extreme precipitation in the Sichuan Basin, and they found that the moisture is mainly concentrated in the middle and lower troposphere and can be tracked to the Arabian Sea. Ren et al. [34] found that the previous SST anomalies in the key areas of the Indian Ocean are closely related to the water vapor over the Tibetan Plateau. In warm water years, significant easterly anomalies near the equator plays a crucial role in the water vapor transport over the plateau in summer. Li et al. [35] discussed the characteristics of abnormal precipitation, large-scale moisture transport, moisture budget, main moisture sources and their contributions in the ESWC from June to July 2020. The results suggested that 70.5% of the local moisture comes from the southern channels such as the Bay of Bengal, South China Sea and Arabian Sea channels, 17.5% is from northern channels, and 11.9% is generated locally. The high sea surface temperature (SST) in the equatorial Middle-East Pacific and the tropical Indian Ocean during the preceding winter contributes to moisture transport to the ESWC.

The above studies mainly focused on the influence of remote moisture transport on precipitation in the ESWC. In addition to the remote moisture transport, the moisture generated by local evaporation can also affect precipitation due to the abundant surface water resources and high summer temperature in the ESWC. The contributions, influencing factors and mechanisms of remote and local evaporation still need to be further studied. This study aims to analyze the contributions of remote moisture transport and local evaporation to the SPE and their possible causes, thereby providing a technical basis for summer precipitation prediction.

The remainder of this paper is organized as follows. Section 2 briefly introduces the data and methods used in this research. Section 3 shows the contributions of remote moisture transport and local evaporation to the climatology of the summer precipitation. Section 4 discusses the contributions of remote moisture transport and local evaporation to interannual and interdecadal variabilities of the summer precipitation. The main conclusions and discussion are presented in section 5.

2 DATA AND METHODS

2.1 *Data*

The precipitation data used in this study is from the daily dataset of basic meteorological elements for China Nation Surface Meteorological Stations (version 3.0) provided by the National Meteorological Information Center of the China Meteorological Administration. The variables in this dataset include air pressure, air temperature, precipitation, evaporation, relative humidity, wind direction and speed, sunshine hours and 0 cm ground temperature for 2474 meteorological

stations in China, and all values have been subjected to strict data quality control. In this study, we select the daily precipitation data of 118 meteorological stations in the ESWC (Fig. 1) from 20: 00 to 20: 00 the next day (Beijing time, the same below) during 1961−2020 for analysis.

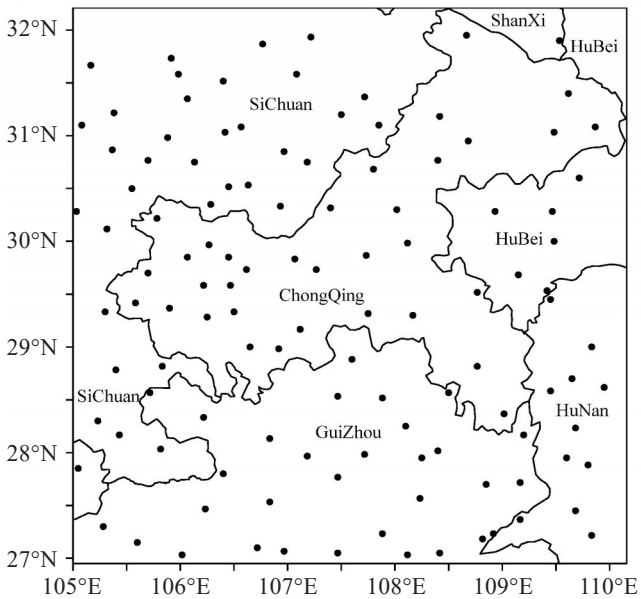

Figure 1. The distribution of 118 meteorological stations over the east of Southwestern China (ESWC).

The atmospheric circulation data adopted in this research are from the daily fifth-generation European Center for Medium-Range Weather Forecasts reanalysis (ERA5) data (Hersbach et al. [36]) from 1961 to 2020, which includes geopotential height, temperature, zonal wind (u), meridional wind (v), vertical velocity (ω), evaporation, precipitation, SST and the integration of moisture flux. The horizontal resolution is 0.25° × 0.25°, and the vertical layers are 37 layers from 1000 hPa to 1 hPa.

The encapsulated National Centers for Environmental Prediction (NCEP) - 1 from the Air Resources Laboratory of the National Oceanic and Atmospheric Administration (Kalnay et al. [37]) is used as forcing data input in the HYSPLIT model (https://www. ready. noaa. gov / archives. php) to simulate moisture trajectories. We select the dataset (four times per day) from 1991 to 2020 for investigation. The variables in this dataset include geopotential height, temperature, zonal wind, meridional wind and vertical velocity, the horizontal resolution is 2.5° × 2.5° , and the vertical layers are 17.

2.2 *Methods*

2.2.1 BRUBAKER'S BINARY MODEL

In this study, Brubaker's binary model based on atmospheric moisture balance (Brubaker et al. [38]; Guo et al. [39]; Li et al. [40]) is adopted to quantitatively describe the contributions of remote moisture transport and local evaporated moisture to precipitation. The calculation method is as follows.

The vertical integration of moisture mass conservation per unit area is shown in Eq. (1).

$$\frac{\partial Q}{\partial t} = -\left(\frac{\partial F_u}{\partial x} + \frac{\partial F_y}{\partial y}\right) + E - P \tag{1}$$

where Q denotes the vertically integrated moisture content (i. e., specific humidity). F_u and F_y indicate the vertically integrated zonal and meridional moisture transport fluxes, respectively. E represents the surface evaporation, and P denotes the precipitation.

If the time scale is sufficiently large (e. g., more than one month) and the variation of moisture with time is negligibly small, $\frac{\partial Q}{\partial t} = 0$.

If the atmosphere is perfectly mixed in the vertical direction over a certain region, and the moisture content (Q_a) from remote moisture transport and the moisture content (Q_e) from local land surface evaporation have an equal opportunity to cause precipitation,

$$\frac{P_a}{P} = \frac{Q_a}{Q} \tag{2}$$

or

$$\frac{P_e}{P} = \frac{Q_e}{Q} \tag{3}$$

where P_a (P_e) represents the precipitation caused by external moisture transport (evaporation).

If E, P and P_a are uniform in the region,

$$\nabla \cdot F\big|_A = F_{out} - F_{in} = (E - P)\,A \tag{4}$$

$$\nabla \cdot F_a\big|_A = F_{a-out} - F_{in} = -P_a A \tag{5}$$

where A indicates the area, $\nabla \cdot F\big|_A$ the convergence and divergence of total moisture in the study area, $\nabla \cdot F_a\big|_A$ the convergence and divergence of the moisture transported to the study area, F_{out} the total moisture flowing out of the study area, F_{a-out} the external input

moisture flowing out of the study area, and F_{in} the total moisture transported to the study area.

If the average moisture flux in the region is the numerical average of the moisture fluxes into and out of the region, the average moisture flux in the region can be written as Eqs. (6–7).

$$\bar{F} = \frac{F_{in} + F_{out}}{2} = F_{in} + \frac{(E - P)A}{2} \tag{6}$$

$$\overline{F_a} = \frac{F_{in} + F_{a-out}}{2} = F_{in} - \frac{P_a A}{2} \tag{7}$$

If the ratio of the moisture advection from outside the area to the moisture generated by local evaporation varies linearly from the upstream to the downstream,

$$\alpha = \frac{P_a}{P} = \frac{\overline{F_a}}{\bar{F}} = \frac{2F_{in}}{EA + 2F_{in}} \tag{8}$$

where α indicates the proportion of the rainfall caused by the external moisture advection to the total rainfall.

$$\alpha_e = \frac{2F_{in-e}}{EA + 2F_{in}}, \alpha_s = \frac{2F_{in-s}}{EA + 2F_{in}}, \alpha_w = \frac{2F_{in-w}}{EA + 2F_{in}}, \alpha_n = \frac{2F_{in-n}}{EA + 2F_{in}} \tag{9}$$

The above equations (Eq. 9) represent the proportions of the precipitation caused by horizontal moisture fluxes entering the area from the eastern (α_e), southern (α_s), western (α_w) and northern (α_n) boundaries to the total precipitation. The precipitation recirculation rate (the ratio of the precipitation caused by local evaporation to the total precipitation) can be expressed by Eq. (10).

$$\rho = 1 - \alpha \tag{10}$$

The precipitation caused by remote moisture transport (P_a) and local evaporation (P_e) is obtained by multiplying the total precipitation P by α and ρ, respectively. The remote moisture flux flowing out of the area (F_{a-out}) and the local evaporated moisture flux flowing out of the area (F_{e-out}) can be expressed by Eq. (11) and Eq. (12), respectively.

$$F_{a-out} = F_{in} - P_a A \tag{11}$$

$$F_{e-out} = F_{out} - F_{a-out} \tag{12}$$

The runoff can be indicated by Eq. (13).

$$R_{runoff} = P - E \tag{13}$$

2.2.2 TRAJECTORY PATTERN

In this study, the Trajstat software (Wang et al. [41]) is used for moisture trajectory analysis, and the HYSPLIT model (Draxler and Hess [42]) is loaded into the software as an external process. By integrating the spatial and temporal position vectors of particle motion trajectories, the HYSPLIT trajectory simulation method can calculate the tracked position of air masses based on the average velocity obtained from the initial position of particles and the first-guess position. Thus, the moisture sources can be obtained by the backward integration of the air mass motion trajectories (Jiang et al. [43]; Zhou et al. [44]).

In this study, we simulate the moisture trajectories (four times per day) from June to August during 1991–2020 (30 years). Due to the huge number of trajectories obtained and the limitation of the software, trajectory clustering is not possible to carry out. Thus, the initial height and point of the simulation are simplified. Since moisture mainly comes from the lower troposphere, the simplified height level of 1500 m (approximately 850 hPa) is taken as the initial height of the simulation. Since there are six grid points in the ESWC on the horizontal resolution of 2.5 ° × 2.5 °, half of them are selected as the initial points of trajectory simulation in the whole simulation space, i.e., the point of 30.00 °N, 105.00 °E, the point of 30.00 °N, 107.50 °E and the point of 30.00 °N, 110.00 °E. Based on this, a three-dimensional motion trajectory tracked backward for 10 days is simulated. The positions of the trajectory points are output once an hour, and the physical attributes (such as temperature, height, air pressure and relative humidity) at the corresponding positions are interpolated. All the initial points of trajectories are tracked backward every 6 hours for 10 days from June to August in 1991–2020. The tracked trajectories, with large numbers, are clustered to determine the final number of trajectories. In addition to clustering the trajectories by using the clustering analysis method (Jiang et al. [43]), the proportion of the contribution of moisture transport in each path is quantified according to the method of Li et al. [35], as shown in Eq. (14).

$$Q_a = \left(\sum_{i=1}^{m} Q_i \Big/ \sum_{j=1}^{n} Q_j\right) \times 100\% \tag{14}$$

where Q_a denotes the proportion of the contribution of moisture transported from a given clustering path, and (Q_i, Q_j) represents the specific humidity at the final location of the path. m indicates the number of trajectories within the path, and n represents the number of total trajectories.

3 CONTRIBUTIONS OF REMOTE MOISTURE TRANSPORT AND LOCAL EVAPORATION TO THE CLIMATOLOGY OF THE SUMMER PRECIPITATION

3.1 *Feasibility analysis of summer precipitation characteristics and ERA5 reanalysis data*

To understand how representative the SPE average series is for the stations in the study area, we calculate the annual average SPE from 1961 to 2020 (Fig. 2a) and its correlation coefficients with the precipitation observations at 118 stations (Fig. 2b). The average SPE is 489.8 mm from 1961 to 2020. As shown in Fig. 2a, the annual average SPE ranges from 387.2 mm to 662 mm, with the highest value in Jianshi County and the lowest value in Gulin County. The rainfall amounts exceed 500 mm in the eastern areas such as Jianshi, Enshi and Xianfeng, in the northern areas such as Xuanhan, Tongjiang and Chengkou, and in the western areas such as Longchang, Xingwen and Naxi. From the distribution of the correlation coefficients between the

annual average SPE series from 1961 to 2020 and the precipitation observation series from 118 stations (Fig. 2b), it can be seen that the correlation coefficients at the vast majority of stations pass the 95% confidence test (above 0.25), and the correlation coefficients at the majority of stations pass the 99.9% confidence test (above 0.489). This result indicates that the annual average SPE series from 1961 to 2020 can generally characterize the precipitation variations in different places.

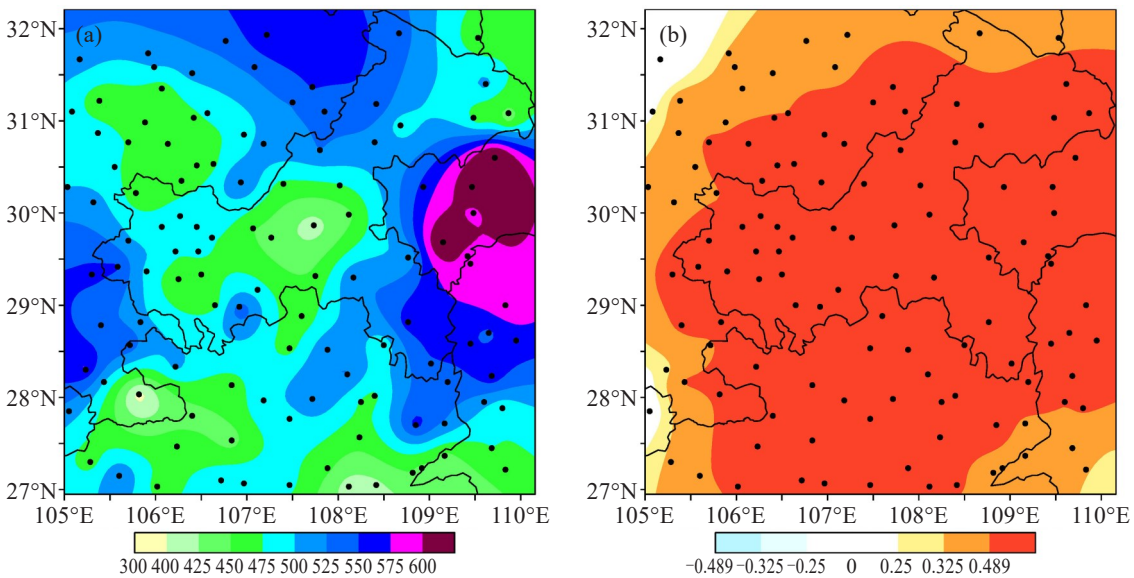

Figure 2. (a) Average summer precipitation (SPE) in the ESWC (units: mm) from 1961 to 2020 obtained in this research and (b) its correlation coefficients with the precipitation observations at 118 stations from 1961 to 2020. The values in the colored areas pass the 95% confidence test.

Since the current observation data cannot provide the variables required for the calculations of Brubaker's binary model, the ERA5 monthly average data is used to analyze the characteristics of precipitation, local evaporation and remote moisture transport in the ESWC and their relationships for more convenient calculation and analysis. Fig. 3 shows the distribution of the correlation coefficients between the average SPE series in 1961−2020 from the ERA5 data and the observations from 118 stations, and the variations of the average SPE from the ERA5 reanalysis data and the observations from 1961 to 2020. As shown in Fig. 3a, the spatial distribution of the ERA5 summer precipitation data is highly consistent with the observations, with large (small) values in the east (west) of the ESWC. Moreover, it is clear that the correlation coefficient distribution of the ERA5 summer precipitation data (multi-year average of 647.8 mm) with the observations at each station (Fig. 3a) is consistent with the distribution pattern in Fig. 2a, and the correlation coefficients at most stations reach 0.64 (passing the 99% confidence test). Although the ERA5 average summer

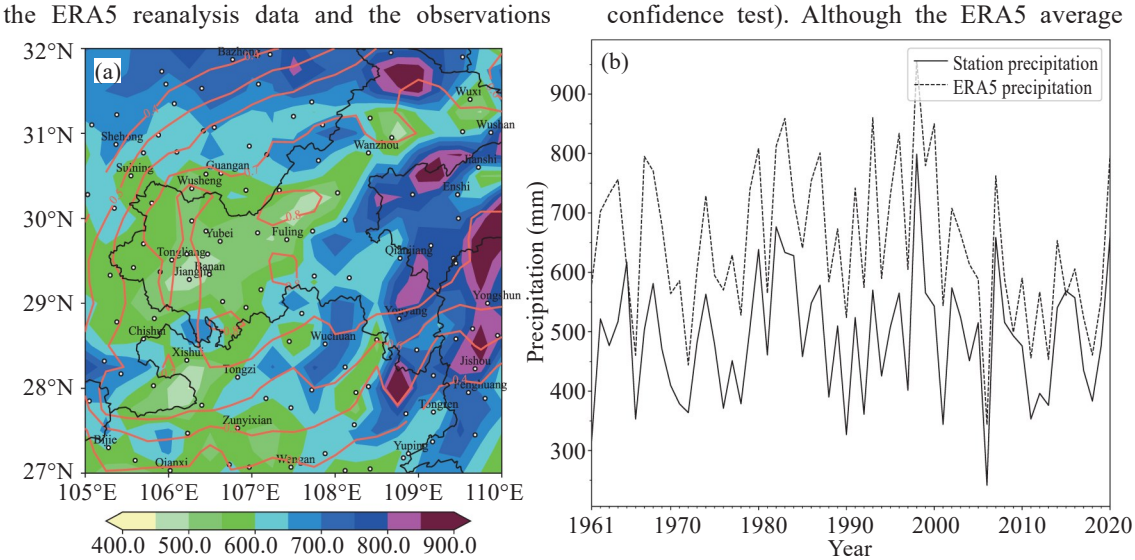

Figure 3. (a) The distribution of the correlation coefficients between the average SPE series from the ERA5 data and observation data at each station, and (b) the variations of the average SPE from the ERA5 data and the observations from 1961 to 2020. The correlation coefficients in colored areas pass the 99% confidence test.

precipitation is larger than the observations, their variations are relatively consistent (Fig. 3b), and their correlation coefficient reaches 0.82 (passing the 99% confidence test). This result indicates that the SPE from the ERA5 data can relatively well describe the characteristics of the observed SPE and is suitable for analyzing precipitation variation patterns.

3.2 *Contribution rates of local evaporation and remote moisture transport to regional precipitation*

Figure 4 presents the average contributions of each member of water cycles to the total SPE from 1961 to 2020 based on the ERA5 data. In terms of the climatic state (Fig. 4), the SPE mainly comes from the contribution of external moisture transport (accounting for 93.59%), while the contribution rate of local evaporation is 6.41%. The remote moisture is 369.96% of the regional rainfall amount, mainly from the southern boundary (292.11%), followed by the western boundary (76.05%) and rarely from the eastern (1.75%) and northern boundaries (0.05%). The moisture from the local evaporation accounts for 50.64% of the regional precipitation. 276.37% of the remote moisture flows out of the study area, while 44.23% of the local evaporated moisture flows out of the area. In total, 49.36% of moisture in the entire area flows out through runoffs.

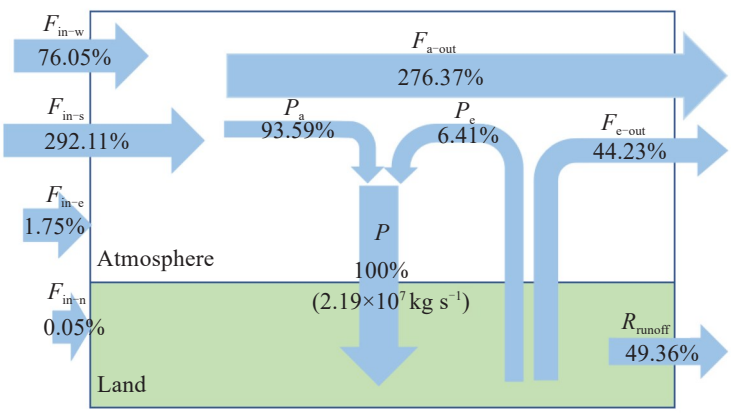

Figure 4. The average contribution of each water cycle member to the total local SPE from 1961 to 2020 (units: %) based on the ERA5 data. P, P_a and P_e indicate the ratios of the local precipitation, remote moisture transport and local evaporation to the total precipitation, respectively, $F_{a\text{-}out}$ ($F_{e\text{-}out}$) denotes the ratio of the outflowing remote moisture flux (evaporation) to the total precipitation, $F_{in\text{-}w}$, $F_{in\text{-}s}$, $F_{in\text{-}e}$, and $F_{in\text{-}n}$ respectively represent the ratios of the moisture from the western, southern, eastern and northern boundaries to the total precipitation, and R_{runoff} indicates the ratio of the runoff (difference between precipitation and evaporation) to the total precipitation.

Table 1 shows the contribution rates of the moisture fluxes from the eastern, southern, western and northern boundaries of Southwest China to the total summer precipitation from 1961 to 2020. In terms of climatic state, the moisture inflow from the southern boundary contributes the most to the summer precipitation (contribution rate of 73.90%), followed by that from the western boundary (contribution rate of 19.24%). The moisture fluxes from the eastern (contribution rate of 0.44%) and northern (contribution rate of 0.01%) boundaries are basically negligible.

Table 1. Contribution rates (%) of the moisture fluxes from eastern, southern, western and northern boundaries to the climatic state of the SPE.

	East boundary	South boundary	West boundary	North boundary
Contribution rate to precipitation (%)	0.44	73.90	19.24	0.01

The distribution of the average vertically integrated moisture fluxes in the summers of 1961–2020 (Fig. 5a) suggests that the moisture transport in the ESWC mainly shows a south-north pattern (slightly eastward). The moisture primarily comes from the southern boundary, with less inflow from the western boundary. The moisture flows outward from the northern and eastern boundaries. From the vertical variations of moisture fluxes at different boundaries (Fig. 5b), it can be found that the moisture transport from the surface to 400 hPa at the southern boundary invariably shows inflow, with the largest inflow in the range of 925–600 hPa. The moisture transport at the western boundary is dominated by inflows above 700 hPa and outflows below 700 hPa. At the eastern and northern boundaries, weak moisture inflows exist in the lower layers (below 850 hPa), and outflows exist above 850 hPa. Since summertime cyclonic circulation controls the Tibetan Plateau, the

associated Tibetan Plateau summer monsoon is active in the middle troposphere (Qi and Li[45]), favoring intensified warm and moist flows into the western boundary above 700 hPa and out of the northern and eastern boundaries above 850 hPa. In contrast, the different moisture transport in the lower troposphere may be due to the interaction between the multi-scale topography of the Sichuan Basin and the different water vapor transport patterns at low latitudes (Li et al. [46]; Qi et al. [47]). Generally, there is more moisture outflow from the eastern boundary.

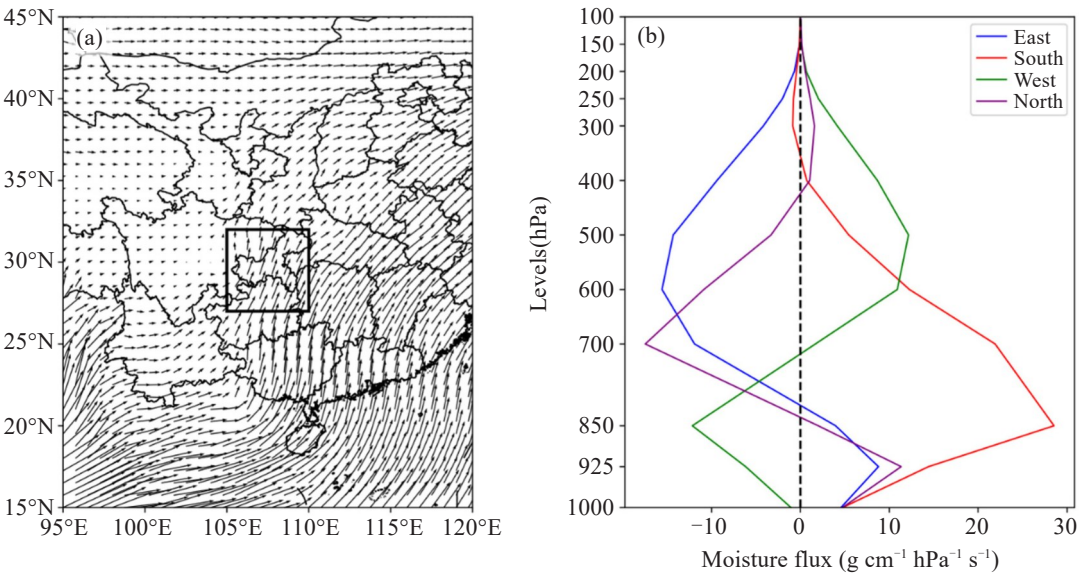

Figure 5. (a) The distribution of the average vertically integrated moisture fluxes in the summers of 1961−2020 and (b) the vertical variations of the moisture flux at each boundary in the ESWC.

To further investigate the paths and contributions of remote moisture transport and analyze the moisture transport characteristics in different channels, we use the HYSPLIT model to simulate the backward trajectories of moisture in the ESWC in the summers of 1991−2020.

A total of 33120 trajectories are obtained by simulating the moisture paths in the summers of 1991−2020 for clustering analysis. Analyzing the growth rates of the spatial variances of trajectories (Fig. 6a), we find that the spatial variances increase rapidly after the number of clusters drops below 5. Thus, the final clustering of simulated trajectory is determined to be 5. Fig. 6b presents the five channels of moisture sources in the ESWC in the summers of 1991−2020. The first one is the Arabian Sea channel, where the moisture mainly comes from the cross-equatorial airflow in Somalia, East Africa and enters the ESWC through the Bay of Bengal and the northern Indochina Peninsula. The second one is the Bay of Bengal channel, where the moisture is mainly from the cross-equatorial airflow in the central and eastern Indian Ocean and then enters the ESWC through the Bay of Bengal and Indochina Peninsula. The third is the western Pacific channel, where the moisture primarily originates from the eastern coast of China and the western Pacific, moves westward from northern Fujian and enters the ESWC after passing through Jiangxi and Hunan Provinces. In the fourth (Northwest channel 1) and fifth (Northwest channel 2) channels, the moisture is mainly from the north. In terms of Northwest channel 1, the moisture mainly comes from West Siberia, reaches Xinjiang through Kazakhstan and then enters the ESWC from Gansu and Sichuan Provinces. In Northwest channel 2, the moisture mainly comes from Mongolia, enters Inner Mongolia from the north and then enters the ESWC through Shaanxi.

In terms of the geopotential height variations (Fig. 6c), the moisture channels, including the Arabian Sea, Bay of Bengal and western Pacific channels, are generally below 900 hPa, all rising to different degrees before entering the ESWC. Specifically, because the Arabian Sea and Bay of Bengal channels pass through the Yunnan-Guizhou Plateau, their geopotential height rises more noticeably, and the moisture is mainly transported to the vicinity of 800 hPa over the ESWC. The geopotential height of Northwest channel 1 displays little variation and is basically stable around 750 hPa, but it decreases slightly after reaching the ESWC. The geopotential height of Northwest channel 2 is near 650 hPa, and it drops markedly after entering the ESWC. Finally, the moisture in this channel converges with that from the Arabian Sea, Bay of Bengal and western Pacific near 800 hPa over Southwest China. The variations of moisture fluxes (Fig. 6d) indicate that the moisture fluxes from low-latitude ocean channels (Arabian Sea channel and Bay of Bengal channel) are obviously larger than those from high-latitude inland

channels (Northwest channels 1 and 2), while the moisture flux from the western Pacific channel is in between. The moisture flux from the Arabian Sea channel increases considerably in the ocean, then enters the land and decreases slightly after crossing the Yunnan-Guizhou Plateau. The moisture fluxes from the other four channels vary slightly with time. The moisture flux from the Bay of Bengal channel decreases slightly after entering the ESWC, while that from Northwest channels 1 and 2 increases slightly. The moisture flux from the western Pacific channel remains basically unchanged.

A comparison of the number of trajectories of each channel finally reaching the ESWC (Table 2) shows that the western Pacific channel has the largest number (10644), followed by the Bay of Bengal channel (10087), the Arabian Sea channel (5698), and the Northwest channel 1 (2518). In terms of the contribution rate of specific humidity of each channel, the Bay of Bengal channel provides the largest contribution, accounting for 33.33%, followed by the western Pacific channel (31.93%), the Arabian Sea channel (19.49%) and the Northwest channel 2 (only 5.09%). In terms of moisture flux contribution rate, the Bay of Bengal Channel again provides the largest contribution, reaching 33.14%, followed by the western Pacific channel (28.86%), the Arabian Sea channel (25.17%) and the Northwest channel 2 (4.30%). Evidently, the number of trajectories from the western Pacific Ocean is the largest, while the Bay of Bengal contributes the largest amount of moisture. A comparison of the five channels shows that the moisture in the ESWC mainly comes from the Bay of Bengal in the summers from 1991 to 2020, followed by the western Pacific Ocean and the Arabian Sea. In addition, Table 2 indicates that the warm and humid moisture with higher potential pseudo-equivalent temperature comes from the ocean (Bay of Bengal, Arabian Sea and western Pacific Ocean), and the dry and cold moisture with lower potential pseudo-equivalent temperature comes from the north.

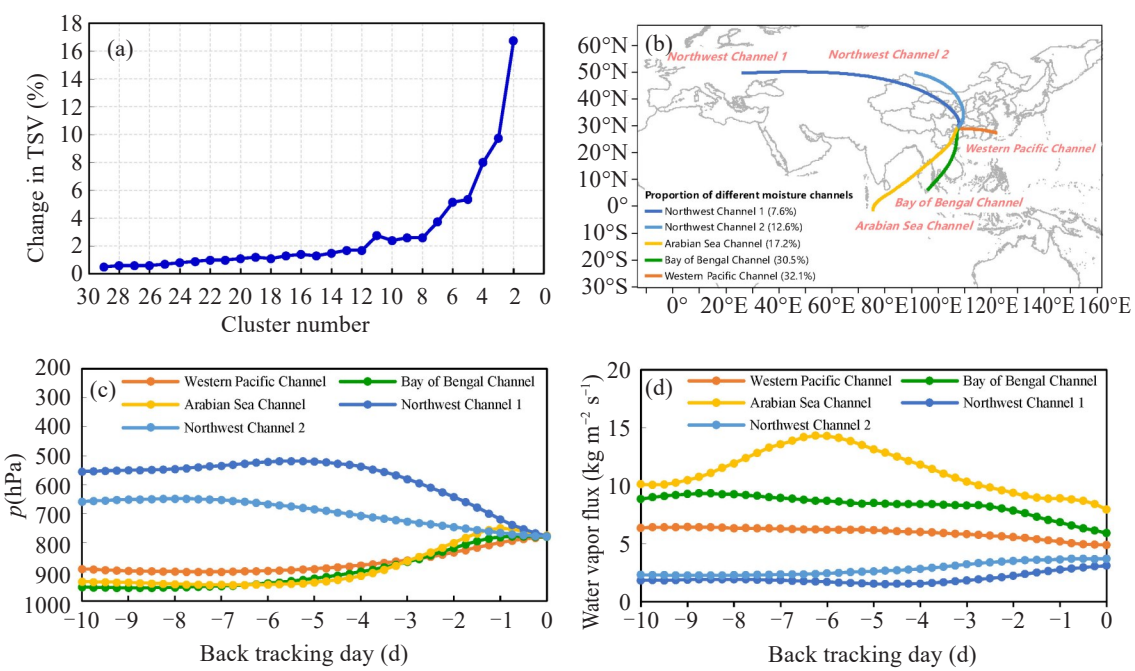

Figure 6. (a) Changes in the TSV (total spatial variance) as clusters combined; (b) spatial distribution of moisture channels; (c) height variations of moisture channels (units: hPa), and (d) changes in the moisture flux of moisture channels (units: kg m^{-2} s^{-1}) in the summers from 1991 to 2020.

Table 2. Total number of trajectories, contributions of specific humidity and moisture flux, and the potential pseudo-equivalent temperature.

Physical quantity	Arabian Sea	Bay of Bengal	Western Pacific	Northwest 1	Northwest 2
Total number of trajectories/tracks	5698	10087	10644	2518	4173
Specific humidity contribution rate/%	19.49	33.33	31.93	5.09	10.16
Moisture flux contribution rate/%	25.17	33.14	28.86	4.30	8.53
Potential pseudo-equivalent temperature/K	348.81	346.40	341.54	329.95	334.09

4 CONTRIBUTIONS OF REMOTE MOISTURE TRANSPORT AND LOCAL EVAPORATION TO INTERANNUAL AND INTERDECADAL VARIABILITIES OF THE SUMMER PRECIPITATION

4.1 *Interannual variability*

To analyze the contributions of remote moisture transport and local evaporation to the interannual variability of SPE, we calculate the regional average precipitation, the precipitation generated by local evaporation, the precipitation generated by remote moisture transport and the interannual variation of precipitation recirculation rate in the ESWC from 1961 to 2020 based on the ERA5 reanalysis data (Fig. 7), as well as the correlation coefficients of each series (Table 3). It is evident that the regional average precipitation is close to and consistent in change with the precipitation produced by remote moisture transport, while the precipitation produced by local evaporation is far less than both. The variation trend of precipitation recirculation rate is opposite to those of the regional average precipitation and the precipitation caused by remote moisture transport, but it is consistent with the variation trend of the precipitation caused by local evaporation. Table 3 shows opposite trends of the regional average precipitation and local evaporation. The regional average precipitation decreases (increases) when the local evaporation increases (decreases). This may be related to the period in summer when there is higher temperature and less precipitation.

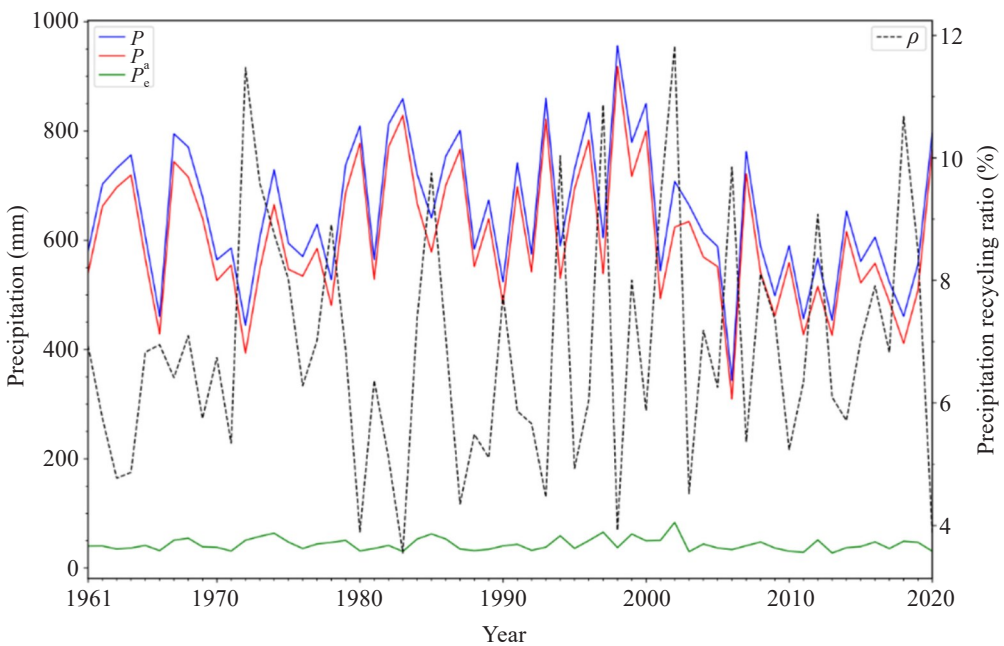

Figure 7. Interannual variations of regional average precipitation (P), the precipitation generated by remote moisture transport (P_a), the precipitation generated by local evaporation (P_e) and the precipitation recirculation rate (ρ) in the ESWC in the summers from 1961 to 2020 calculated based on ERA5 reanalysis data.

Table 3. Correlation coefficients between P (the regional average precipitation), E (the local evaporation), P_a (the precipitation generated by remote moisture transport), P_e (the precipitation generated by local evaporation), α (the proportion of precipitation generated by remote moisture transport to the total precipitation), and ρ (the precipitation recirculation rate) calculated based on ERA5 reanalysis data from 1961 to 2020. The blue color indicates that the number has passed the 99% confidence test).

	P	E	P_a	P_e	α	ρ
P	1.0	−0.57	0.99	0.13	0.54	−0.54
E	−0.57	1.0	−0.59	0.17	−0.49	0.49
P_a	0.99	−0.59	1.0	0.04	0.61	−0.61
P_e	0.13	0.17	0.04	1.0	−0.74	0.74
α	0.54	−0.49	0.61	−0.74	1.0	1.0

Figure 8 shows the contribution rate of the moisture transport from four boundaries to the average precipitation in the ESWC and the interannual variation of precipitation anomaly percentage calculated based on ERA5 reanalysis data in the summers from 1961 to 2020. As can be seen, the contribution rate of moisture transport to precipitation from the south boundary is the largest every year, followed by that from the west boundary, while the contribution from the north boundary is almost none. The contribution rate from the east boundary is also very small except in 1994 and 2018 when it nearly reaches 20%, and the reason needs to be discussed in future. The correlation coefficient of each series (Table 4) suggests close relations between the regional average precipitation and the moisture transport contribution rate from the west boundary. When the contribution rate from the west boundary increases, there tends to be more precipitation in the ESWC, and vice versa. However, the change in regional average precipitation is not closely related to the contributions from the other three boundaries. The contribution rate of moisture transport from the west boundary exhibits an opposite trend to that from the east and south boundaries. When the contribution rate from the west boundary increases, the contribution rate from the east and south boundaries will decrease, and vice versa.

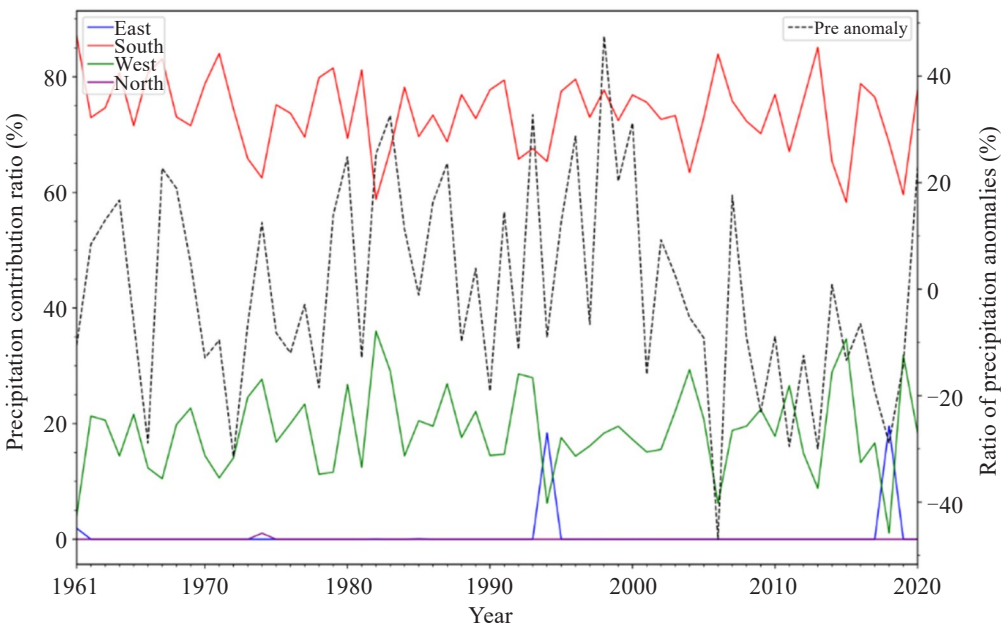

Figure 8. Interannual variation of contribution rate of moisture transport from four boundaries to the regional average precipitation and the precipitation (abbreviated as "Pre" in the figure) anomaly percentage in the ESWC in the summers from 1961 to 2020 calculated based on the ERA5 reanalysis data.

Table 4. The correlation coefficients of the contribution rate of moisture transport from four boundaries to the average precipitation and the interannual variation of precipitation anomaly percentage in the ESWC in the summers from 1961 to 2020 calculated based on ERA5 reanalysis data. The blue color indicates that the number has passed the 99% confidence test.

	Precipitation anomaly percentage	East boundary	South boundary	West boundary
East boundary	−0.19	1.0	−0.17	−0.41
South boundary	−0.10	−0.17	1.0	−0.79
West boundary	0.32	−0.41	−0.79	1.0
North boundary	0.09	−0.03	−0.24	0.18

4.2 *Interdecadal variability*

To analyze the contributions of remote moisture transport and local evaporation to the interdecadal variability of SPE, the regional average precipitation anomaly percentage, the precipitation generated by moisture transport at each boundary and the contribution rate of local evaporation to the SPE from 1961 to 2020 are calculated based on ERA5 reanalysis data (Table 5).

As can be seen, the SPE is generally larger in the 1960s, 1980s and 1990s, especially in 1990s, but smaller in the 1970s, 2000s and 2010s. The south boundary contributes the most moisture transport, followed by the west boundary, while the east and north boundaries make basically negligible contributions. The contribution rate of local evaporation is about 7%. In terms of the contributions of external input and local evaporation, the years with more summer precipitation correspond to the higher external input. The contribution rate of local evaporation shows an opposite trend, with relatively high contribution rate in the years with less precipitation (above 7%). This result shows that when there is more precipitation, there is usually relatively high contribution rate of external input moisture and relatively low contribution rate of local evaporation, and vice versa. The reason may be that the increase of evaporation is caused by limited rainfall and higher temperature in summer.

Table 5. Average contribution rate of local evaporation and moisture flux inflow from the east, south, west and north boundaries to the SPE (units: %).

Decade	Percentage of summer precipitation anomaly	East boundary	South boundary	West boundary	North boundary	External input	Local evaporation
1961−1970	2.62%	0.19%	77.41%	16.19%	0.00%	93.79%	6.21%
1971−1980	−3.79%	0.00%	73.60%	18.68%	0.10%	92.38%	7.62%
1981−1990	7.03%	0.01%	72.48%	21.31%	0.01%	93.81%	6.19%
1991−2000	16.08%	1.84%	73.52%	18.07%	0.00%	94.06%	6.57%
2001−2010	−8.90%	0.00%	73.72%	18.78%	0.00%	92.50%	7.50%
2011−2020	−13.04%	1.96%	71.32%	19.52%	0.00%	92.80%	7.20%

4.3 *Possible causes of the contributions of remote moisture transport and local evaporation to the interannual variability of SPE*

The contributions of remote moisture transport and local evaporation to the interannual variability of SPE is mainly affected by atmospheric circulation and external forcing. The ERA5 reanalysis data from 1961 to 2020 is used to calculate the regression coefficients of standardized series of regional average precipitation anomalies and the contribution rate series of local evaporation against the vertically integrated moisture flux, 700 hPa and 200 hPa vertical velocity, 850 hPa wind, 500 hPa potential height and SST (Fig. 9). In the years with more precipitation (with higher contribution rate of remote moisture transport), there are obvious anticyclonic circulation anomalies of moisture transport in the ESWC and its vicinity, with considerably stronger integrated moisture transport in the southwest-northeast direction (Fig. 9a). At 850 hPa, obvious southwesterly wind anomalies are observed (Fig. 9b). Updraft prevails in the ESWC from 700 hPa (Fig. 9c) to 200 hPa (Fig. 9d). In the 500 hPa height field, the "+ − +" anomaly distribution appears prominently in East Asia, with a more southerly western Pacific subtropical high and double blocking highs in mid-high latitudes (Fig. 9e). The above anomalous circulation configuration indicates a possible cooperation between the mid-latitude Rossby wave train-like teleconnection (e.g silk road pattern, Lu et al. [48]) and the East Asia and Pacific pattern (Huang and Li [49]).

The years with more SPE correspond to relatively high SST in the equatorial Middle East Pacific, the South China Sea, the Bay of Bengal, the Arabian Sea and other places (Fig. 9f). In case of higher contribution rate of local evaporation (overly higher precipitation recirculation rate), there are obvious cyclonic circulation anomalies of moisture transport in the ESWC and its vicinity, with considerably weaker integrated moisture transport in a southwest-northeast orientation (Fig. 9g). At 850 hPa, obvious northeasterly wind anomalies are observed (Fig. 9h). From 700 hPa (Fig. 9i) to 200 hPa (Fig. 9j), downward motion prevails. In the 500 hPa height field, the "− + −" anomaly distributions are obvious in East Asia, with a northerly western Pacific subtropical high (Fig. 9k). In the equatorial Middle East Pacific, the South China Sea, the Bay of Bengal and the Arabian Sea the SST is relatively low (Fig. 9l). Overall, this is a typical circulation configuration for less summer precipitation in Southwest China (Li et al. [50]).

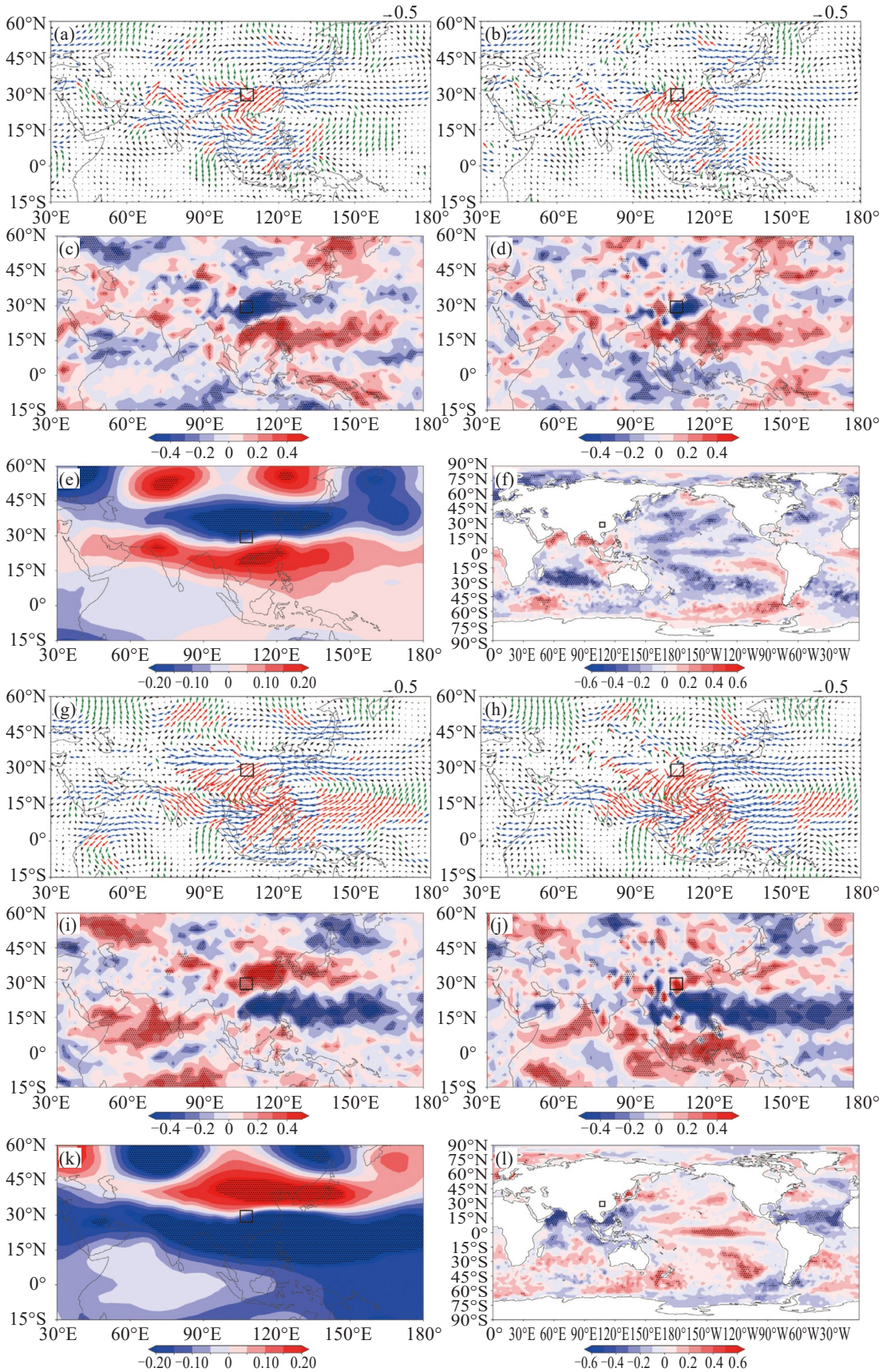

Figure 9. Regression coefficients of standardized series of regional average precipitation anomalies and contribution rate series of local evaporation against vertically integrated moisture flux (a, g), 850 hPa wind field (b, h), 200 hPa (c, i) and 700 hPa (d, j) vertical velocity field, 500 hPa geopotential height field (e, k), and SST (f, l). The dotted areas in the graph indicate that the regression coefficients have passed the 90% confidence test, and the red, blue and green arrows in the wind vector graph indicate that the results have passed the 90% confidence test in the *uv* direction, *u* direction and *v* direction.

5 CONCLUSIONS AND DISCUSSION

The following conclusions are drawn from the analyses of remote moisture transport, local evaporation and their contributions to SPE.

In terms of the climatology, the SPE is mainly contributed by the external transport (93.59%), while the local evaporation contributes only 6.41%. In summer, the moisture inflow from the south boundary contributes the most (73.90%), followed by that from the west boundary (19.24%), while the contribution of moisture inflow from the east and north boundaries is basically negligible.

There are five remote moisture channels for the SPE, i. e., the Arabian Sea channel, the Bay of Bengal channel, the western Pacific channel, the Northwest channel 1 and channel 2. Among the five channels, the western Pacific channel has the largest number of trajectories (10644), and the Northwest channel 1 has the least (2518). In terms of specific humidity contribution rate, the Bay of Bengal channel contributes the most (33.33%). In summer, the moisture in the ESWC mainly comes from the Bay of Bengal, followed by the western Pacific Ocean and the Arabian Sea.

The variation of precipitation recirculation rate is opposite to that of regional average precipitation and the precipitation caused by remote moisture transport, but consistent with that of the precipitation caused by local evaporation. When local evaporation increases (decreases), the regional precipitation declines (rises). The change of regional average precipitation is closely related to the contribution rate of moisture transport from the west boundary. When the latter increases, the possibility of more precipitation rises, and vice versa.

A comparison of the contributions of external input and local evaporation in different years shows that the years with more SPE correspond to larger external moisture input. The opposite trend is observed in local evaporation. In a word, more precipitation corresponds to larger contributions of external moisture input and smaller contributions of local evaporation.

In the years with more SPE (higher contribution rate of remote moisture transport), there is obvious southwest-northeast oriented moisture transport and deep updrafts in the ESWC. Meanwhile, there is a "+ − + " height anomaly wave train in East Asia, a southerly western Pacific subtropical high, double blocking in mid-high latitudes, and high SST in the equatorial Middle East Pacific and South China Sea. All the circulation configuration is beneficial to the moisture transport from southwest to the study area.

This study analyzes the moisture sources and their contributions to the SPE and discusses the possible causes of the interannual variation of the contribution rate of remote moisture and local evaporation. Further analysis is needed on predicting the summer precipitation to explore the mechanism of how external forcing factors such as preceding SST and plateau snow cover impact the moisture transport and precipitation in the ESWC.

***Acknowledgements*:** We thank the two anonymous reviewers for their considerable contribution to the publication of this paper.

REFERENCES

[1] LI Y Q. Surface heating in the Tibetan Plateau and general circulation over it and their relations with the prediction of Drought-Flood at its eastern side [J]. Chinese Journal of Atmospheric Sciences, 2003, 21(1): 107-114 (in Chinese), https://doi.org/10.3878/j.issn.1006-9895.2003.01.10

[2] MA Z F, TAN Y B. A physical statistic model for predicting the rainfall during flood season in Sichuan-Chongqing region [J]. Chinese Journal of Atmospheric Sciences, 2004, 28(1): 138-145 (in Chinese), https://doi. org / 10.3878 / j. issn.1006-9895.2004.01.13

[3] WU G X. Atmospheric transports and budgets of water vapour and their impacts on subtropical drought [J]. Chinese Journal of Atmospheric Sciences, 1990, 14(1): 53-63 (in Chinese), https://doi. org / 10.3878 / j. issn. 1006-9895.1990.01.08

[4] ZHAI P M, ESKRIDGE R E. Atmospheric water vapor over China [J]. Journal of Climate, 1997, 10(10): 2643-2652, https://doi. org / 10.1175 / 1520-0442(1997)010<2643: AWVOC>2.0.CO;2

[5] HUANG R H, ZHANG Z Z, HUANG G, et al. Characteristics of the water vapor transport in East Asian monsoon region and its difference from that in South Asian monsoon region in summer [J]. Chinese Journal of Atmospheric Sciences, 1998, 22(4): 460-469 (in Chinese), https://doi.org/10.3878/j.issn.1006-9895.1998.04.08

[6] ZHANG R H. Relations of water vapor transport from Indian monsoon with that over East Asia and the summer rainfall in China [J]. Advances in Atmospheric Sciences, 2001, 18(5): 1005-1017, https://doi. org / 10.1007 / BF03403519

[7] ZHOU C Y, LI Y Q. Climatological characteristics of water vapor transport over upstream area of Yangtze river [J]. Journal of Yangtze River Scientific Research Institute, 2005, 22(5): 18-22 (in Chinese).

[8] HE J H, SUN C H, LIU Y Y, et al. Seasonal transition features of large-scale moisture transport in the Asian-Australian Monsoon region [J]. Advances in Atmospheric Sciences, 2007, 24(1): 1-14, https://doi. org / 10.1007 / S00376-007-0001-5

[9] ZHANG X D, HE J X, ZHANG J, et al. Enhanced poleward moisture transport and amplified northern high-latitude wetting trend [J]. Nature Climate Change, 2013, 3 (1): 47-51, https://doi.org/10.1038/NCLIMATE1631

[10] RYU Y H, SMITH J A, BOU-ZEID E. On the climatology of precipitable water and water vapor flux in the mid-Atlantic region of the United States [J]. Journal of Hydrometeorology, 2015, 16(1): 70-87, https://doi. org / 10.1175/JHM-D-14-0030.1

[11] WANG X L, DING Y H, ZHANG Q Y. Circulation pattern and moisture transport for summertime persistent heavy precipitation in eastern China [J]. Climatic and Environmental Research, 2017, 22(2): 221-230 (in

Chinese), https://doi. org / 10.3878 / j. issn. 1006-9585.2016.16056

[12] LI X R, FAN K, XU Z Q. Decrease in extreme precipitation in summer over east northern China and the water-vapor transport characteristics after year 2000 [J]. Chinese Journal of Atmospheric Sciences, 2019, 43(5): 1109-1124 (in Chinese), https://doi. org / 10.3878 / j. issn.1006-9895.1902.18198

[13] SUN B, WANG H J, ZHOU B T, et al. A review on the interannual and interdecadal variations of water vapor transport over China during past decades [J]. Advances in Water Science, 2020, 31(5): 644-653 (in Chinese), https://doi.org/10.14042/j.cnki.32.1309.2020.05.002

[14] TAO S Y, ZHAO Y J, CHEN X M. The relationship between May-Yü in Far East and the behavior of circulation over Asia [J]. Acta Meteorologica Sinica, 1958, 29(2): 119-134 (in Chinese), https://doi. org / 10.11676/qxxb1958.014

[15] XIE Y B, DAI W J. Certain computational results of water vapor transport over eastern China for a selected synoptic case [J]. Acta Meteorologica Sinica, 1959, 30(2): 171-185 (in Chinese), https://doi.org/10.11676/qxxb1959.021

[16] DING Y H, HU G Q. A study on water vapor budget over China during the 1998 severe flood periods [J]. Acta Meteorologica Sinica, 2003, 61(2): 129-145 (in Chinese), https://doi.org/10.11676/qxxb2003.014

[17] XU X D, CHEN L S, WANG X R, et al. Source-sink structure of water vapor transport in Meiyu belt of Yangtze River basin [J]. Chinese Science Bulletin, 2003, 48(21): 2288-2294 (in Chinese), https://doi.org/10.1360/csb2003-48-21-2288

[18] MA J J, GAO X Q. The transportation paths of water vapor and its relation to climate change over North China [J]. Plateau Meteorology, 2006, 25(5): 893-899 (in Chinese).

[19] JIANG Z H, REN W, LIU Z Y, et al. Analysis of water vapor transport characteristics during the Meiyu over the Yangtze-Huaihe River vally using the Lagrangian method [J]. Acta Meteorologica Sinica, 2013, 71(2): 295-304 (in Chinese), https://doi.org/10.11676/qxxb2013.017

[20] YANG L, ZHAO J H, FENG G L. Characteristics and differences of summertime moisture transport associated with four rainfall patterns over eastern China monsoon region [J]. Chinese Journal of Atmospheric Sciences, 2018, 42(1): 81-95 (in Chinese), https://doi.org/10.3878/j.issn.1006-9895.1706.16273

[21] CHU Q C, ZHI R, WANG Q G, et al. Roles of moisture sources and transport in precipitation variabilities during boreal summer over East China [J]. Climate Dynamics, 2019, 53(9-10): 5437-5457, https://doi. org / 10.1007 / s00382-019-04877-z

[22] CHU Q C, WANG Q G, FENG G L. The roles of moisture transports in intraseasonal precipitation during the preflood season over South China [J]. International Journal of Climatology, 2020, 40(4): 2239-2252, https://doi.org/10.1002/joc.6329

[23] LI Y Q, JIANG X W. Characteristics of water vapor transportation during summer heavy rainfall at the upper reaches of Yangtze River in 1998 [J]. Torrential Rain and Disasters, 2007, 26(1): 37-41 (in Chinese).

[24] CHEN B, XU X D, SHI X H. Estimating the water vapor transport pathways and associated sources of water vapor for the extreme rainfall event over east of China in July 2007 using the Lagrangian method [J]. Acta Meteorologica Sinica, 2011, 69(5): 810-818 (in Chinese), https://doi.org/10.11676/qxxb2011.071

[25] DING Y H, LIU Y J, SONG Y F. East Asian summer monsoon moisture transport belt and its impact on heavy rainfalls and floods in China [J]. Advances in Water Science, 2020, 31(5): 629-643 (in Chinese), https://doi.org/10.14042/j.cnki.32.1309.2020.05.001

[26] RAN L K, LI S W, ZHOU Y S, et al. Observational analysis of the dynamic, thermal, and water vapor characteristics of the "7.20" extreme rainstorm event in Henan Province, 2021 [J]. Chinese Journal of Atmospheric Sciences, 2021, 45(6): 1366-1383 (in Chinese), https://doi. org / 10.3878 / j. issn. 1006-9895.2109.2116

[27] SUN Y, XIAO H, YANG H L, et al. Analysis of dynamic conditions and hydrometeor transport of Zhengzhou superheavy rainfall event on 20 July 2021 based on optical flow field of remote sensing data [J]. Chinese Journal of Atmospheric Sciences, 2021 45(6): 1384-1399 (in Chinese), https://doi. org/ 10.3878 / j. issn. 1006-9895.2109.21155

[28] BUEH C L, ZHUGE A R, XIE Z W, et al. Water vapor transportation features and key synoptic-scale systems of the "7.20" rainstorm in Henan Province in 2021 [J]. Chinese Journal of Atmospheric Sciences, 2022, 46(3): 725-744 (in Chinese), https://doi.org/10.3878/j.issn.1006-9895.2202.21226

[29] ZHOU C Y, LI Y Q, LI W, et al. Climatological characteristics of water vapor transport over eastern part of Qinghai-Xizang Plateau and its surroundings [J]. Plateau Meteorology, 2005, 24(6): 880-888 (in Chinese).

[30] JIANG X W, LI Y Q, LI C, et al. Characteristics of summer water vapor transportation in Sichuan Basin and its relationship with regional drought and flood [J]. Plateau Meteorology, 2007, 26(3): 476-484 (in Chinese).

[31] LI Y H, XU H M, GAO Y H, et al. The characteristics of moisture transport associated with drought / flood in summer over the east of the southwestern China [J]. Acta Meteorologica Sinica, 2010, 68(6): 932-943 (in Chinese), https://doi.org/10.11676/qxxb2010.088

[32] LI C S, TANG D C, SONG P. Study on influences of abnormal moisture transport in Southwest China [J]. Journal of Catastrophology, 2012, 27(4): 28-33 (in Chinese).

[33] HUANG Y J, CUI X P. Moisture sources of an extreme precipitation event in Sichuan, China, based on the Lagrangian method [J]. Atmospheric Science Letters, 2015, 16(2): 177-183, https://doi.org/10.1002/asl2.562

[34] REN Q, ZHOU C Y, HE J H, et al. Impact of preceding Indian Ocean sea surface temperature anomaly on water vapor content over the Tibetan Plateau moist pool in summer and its possible reason [J]. Chinese Journal of Atmospheric Sciences, 2017, 41 (3): 648-658 (in Chinese), https://doi. org / 10.3878 / j. issn. 1006-9895.1610.16161

[35] LI Y H, ZHOU J, HE J X, et al. Characteristics of water vapor transport associated with abnormal precipitation over the east of southwestern China in June and July 2020 [J]. Chinese Journal of Atmospheric Sciences, 2022, 46 (2): 309-326 (in Chinese), https://doi. org / 10.3878 / j.

issn.1006-9895.2105.21002

[36] HERSBACH H, BELL B, BERRISFORD P, et al. The ERA5 global reanalysis [J]. Quarterly Journal of the Royal Meteorological Society, 2020, 146(730): 1999-2049, https://doi.org/10.1002/qj.3803

[37] KALNAY E, KANAMITSU M, KISTLER R, et al. The NCEP / NCAR 40-year reanalysis project [J]. Bulletin of the American Meteorological Society, 1996, 77(3): 437-472, https://doi. org / 10.1175 / 1520-0477(1996)077<0437: TNYRP>2.0.CO;2

[38] BRUBAKER K L, ENTEKHABI D, EAGLESON P S. Estimation of continental precipitation recycling [J]. Journal of Climate, 1993, 6(6): 1077-1089, https://doi.org/10.1175/1520-0442(1993)006<1077:EOCPR>2.0.CO;2

[39] GUO L, KLINGAMAN N P, DEMORY M E, et al. The contributions of local and remote atmospheric moisture fluxes to East Asian precipitation and its variability [J]. Climate Dynamics, 2018, 51(11-12): 4139-4156, https://doi.org/10.1007/s00382-017-4064-4

[40] LI Y S, ZHANG L X, WANG B. Contributions of local and remote water vapor transport to precipitation variations over Songhua River basin [J]. Chinese Journal of Atmospheric Sciences, 2020, 44(3): 611-624 (in Chinese), https://doi. org / 10.3878 / j. issn. 1006-9895.1909.19177

[41] WANG Y Q, ZHANG X Y, DRAXLER R R. TrajStat: GIS-based software that uses various trajectory statistical analysis methods to identify potential sources from long-term air pollution measurement data [J]. Environmental Modelling and Software, 2009, 24(8): 938-939, https://doi.org/10.1016/j.envsoft.2009.01.004

[42] DRAXLER R R, HESS G D. An overview of the HYSPLIT_4 modeling system for trajectories, dispersion and deposition [J]. Australian Meteorological Magazine, 1998, 47(4): 295-308.

[43] JIANG Z H, LIANG Z R, LIU Z Y, et al. A diagnostic study of water vapor transport and budget during heavy precipitation over the Huaihe River Basin in 2007 [J]. Chinese Journal of Atmospheric Sciences, 2011, 35(2): 361-371 (in Chinese), https://doi.org/10.3878/j.issn.1006-9895.2011.02.14

[44] ZHOU Y S, YAN L, WU T Y, et al. Comparative analysis of two rainstorm processes in Sichuan Province affected by the Tibetan Plateau vortex and Southwest vortex [J]. Chinese Journal of Atmospheric Sciences, 2019, 43(4): 813-830 (in Chinese), https://doi.org/10.3878/j.issn.1006-9895.1807.18147

[45] QI D M, LI Y Q. The major progress of the Plateau monsoon study and its scientific significance [J]. Arid Meteorology, 2007, 25(4): 74-79 (in Chinese).

[46] LI Y Q, LI D J, YANG S, et al. Characteristics of the precipitation over the eastern edge of the Tibetan Plateau [J]. Meteorology and Atmospheric Physics, 2010, 106(1-2): 49-56, https://doi.org/10.1007/S00703-009-0048-1

[47] QI D M, LI Y Q, ZHOU C Y. Variation characteristics of summer water vapor budget and its relationship with the precipitation over the Sichuan Basin [J]. Water, 2021, 13 (18): 2533, https://doi.org/10.3390/w13182533

[48] LU R Y, OH J H, KIM B J. A teleconnection pattern in upper-level meridional wind over the North African and Eurasian continent in summer [J]. Tellus A: Dynamic Meteorology and Oceanography, 2002, 54(1), 44-55, https://doi.org/10.3402/tellusa.v54i1.12122

[49] HUANG R H, LI W J. Influence of heat source anomaly over the western tropical Pacific on the subtropical high over East Asia and its physical mechanism [J]. Chinese Journal of Atmospheric Sciences, 1988, 12(s1): 107-116 (in Chinese), https://doi. org / 10.3878 / j. issn. 1006-9895.1988.t1.08

[50] LI Y H, XU H M, LIU D. Features of the extremely severe drought in the east of South China and anomalies of atmospheric circulation in summer 2006 [J]. Acta Meteorological Sinia, 2009, 67(1): 122-132 (in Chinese), https://doi.org/10.11676/qxxb2009.013

Citation: LI Yong-hua, HUANG Ding-an, LU Chu-han, et al. Moisture Sources and Their Contributions to Summer Precipitation in the East of Southwest China [J]. Journal of Tropical Meteorology, 2023, 29(2): 153-167, https://doi. org / 10.46267 / j. 1006-8775.2023.012